Review Article

Assessing tissue metabolism by phosphorous-31 magnetic resonance spectroscopy and imaging: a methodology review

Yuchi Liu[1], Yuning Gu[1], Xin Yu[1,2,3,4]

[1]Department of Biomedical Engineering, [2]Department of Radiology, [3]Department of Physiology and Biophysics, [4]Case Center for Imaging Research, Case Western Reserve University, Cleveland, OH, USA

Correspondence to: Xin Yu, ScD. Wickenden 430, 10900 Euclid Avenue, Cleveland, OH 44106, USA. Email: xin.yu@case.edu.

Abstract: Many human diseases are caused by an imbalance between energy production and demand. Magnetic resonance spectroscopy (MRS) and magnetic resonance imaging (MRI) provide the unique opportunity for *in vivo* assessment of several fundamental events in tissue metabolism without the use of ionizing radiation. Of particular interest, phosphate metabolites that are involved in ATP generation and utilization can be quantified noninvasively by phosphorous-31 (^{31}P) MRS/MRI. Furthermore, ^{31}P magnetization transfer (MT) techniques allow *in vivo* measurement of metabolic fluxes via creatine kinase (CK) and ATP synthase. However, a major impediment for the clinical applications of ^{31}P-MRS/MRI is the prohibitively long acquisition time and/or the low spatial resolution that are necessary to achieve adequate signal-to-noise ratio. In this review, current ^{31}P-MRS/MRI techniques used in basic science and clinical research are presented. Recent advances in the development of fast ^{31}P-MRS/MRI methods are also discussed.

Keywords: Magnetization transfer (MT); creatine kinase (CK); ATP synthesis; mitochondrial function

Submitted Oct 03, 2017. Accepted for publication Nov 11, 2017.
doi: 10.21037/qims.2017.11.03
View this article at: http://dx.doi.org/10.21037/qims.2017.11.03

Introduction

Most cellular processes require energy to be carried out. Adenosine triphosphate (ATP), often referred to as the energy currency in living organisms, is critically important for maintaining normal cellular functions. There is increasing recognition that many human diseases are caused by an imbalance between ATP production and demand (1,2). Magnetic resonance spectroscopy (MRS) and magnetic resonance imaging (MRI) provide powerful tools for *in vivo* assessment of tissue metabolism without ionizing radiation. The noninvasive nature of these techniques enables repeated measurements such that disease progression and treatment response can be monitored longitudinally. Of particular interest, phosphorous-31 (^{31}P) MRS and MRI allow the evaluation of several important aspects of high-energy phosphate metabolism, from metabolite concentrations to metabolic fluxes through ATP-generating enzymes. Since 1970s, numerous studies have employed ^{31}P-MRS/MRI in the investigation of a broad range of diseases such as diabetes, stroke, heart failure, and cancers (3-8). These studies have provided invaluable insights into the role of mitochondrial metabolism in normal physiology and disease development.

A major impediment that has hampered the clinical use of ^{31}P-MRS/MRI is the low sensitivity of ^{31}P nuclei. Because of the extremely low concentrations of phosphate metabolites, current ^{31}P-MRS/MRI methods require prohibitively long acquisition time to achieve adequate signal-to-noise ratio (SNR), which is not practical for routine use on clinical patients. As a result, ^{31}P-MRS/MRI has found limited clinical applications, especially in evaluating the heterogeneity in metabolic alterations. Although the increased use of high field scanners in recent years is promising to significantly improve SNR for imaging ^{31}P metabolites with high spatial resolution (9), fast ^{31}P-MRS/MRI methods capable of

mapping phosphate metabolites and metabolic fluxes are still highly desired for metabolic evaluations.

This article provides an overview of ^{31}P-MRS/MRI methods with a focus on techniques for spatial localization, metabolic mapping, and recent development in fast ^{31}P-MRS/MRI techniques. Applications of these techniques to the investigation of a specific physiology/pathology will be discussed without detailed description. Interested readers are referred to recent review articles on the applications of ^{31}P-MRS/MRI in metabolic characterization of skeletal muscle (10-12), heart (13), brain (14), and liver (11), as well as in diseases such as cancer (15), heart failure (16), and obesity and diabetes (17,18).

Historical perspective

The use of ^{31}P-MRS for metabolic investigations dates back to 1960. Cohn and Hughes were the first to obtain a high-resolution ^{31}P spectrum of a solution of ATP (19). In addition, they also observed a dependence of the chemical shifts of the phosphorus nuclei of ATP on the pH of the solution. In parallel to the early development of MRI methods by Lauterbur (20), the entire 1970s also witnessed the rapid advance of ^{31}P-MRS in metabolic investigation of a broad range of biological systems. In 1973, Moon and Richards performed the first ^{31}P-MRS study that measured intracellular pH in human red blood cells (21). In the following year, Henderson and colleagues obtained the first ^{31}P spectrum of ATP from human red blood cells (22). At the same time, the Oxford team led by Radda performed the first experiment to acquire ^{31}P spectra from an intact organ, i.e., the excised and superfused muscle of rat hindlimb (23). The first *in vivo* ^{31}P-MRS study was performed on mouse brain by Chance *et al.* (24). Within the short span of one decade, organelles including mitochondria (25,26) and chromaffin granules (27), cells including *Escherichia coli* (28), yeast (29), and hepatocytes (30), and organs including skeletal muscle (31,32), heart (33-35), brain (36), kidney (37), and liver (38,39) have all been studied using ^{31}P-MRS. It is worth noting that most of these organ studies were performed on excised organs to avoid the need for spatial localization. Although Lauterbur has demonstrated the feasibility of imaging water protons (20), it was considered impractical for ^{31}P imaging of living systems because of the low sensitivity and difficulties with spectral resolution.

The 1980s began with the publication of two important studies that aimed at acquiring ^{31}P spectra from spatially defined regions *in vivo*. Ackerman *et al.* were the first to use a surface coil for detecting ^{31}P signal in localized regions adjacent to the coil (40). By taking advantage of the sensitive volume of a surface coil, they were able to acquire ^{31}P spectra from rat leg and brain *in vivo* without the use of spatial localization sequences. Due to the simplicity of such an approach, as well as the high sensitivity of surface coils, surface coils are still used in many spectroscopic studies nowadays. However, a fundamental limitation for this approach is that it cannot be adopted for detecting signals from internal organs noninvasively. At the same time, Bendel *et al.* demonstrated for the first time the feasibility of spatial mapping of phosphate metabolites in a phantom comprised of ATP, phosphocreatine (PCr), and inorganic phosphate (P_i) (41). Later, Bottomley *et al.* proposed the Depth-REsolved Surface coil Spectroscopy (DRESS) method to acquire one-dimensional localized ^{31}P spectra using a surface coil (42,43). This technique has been widely used in evaluating myocardial metabolism (44,45) and the bioenergetics of skeletal muscle (46). Several single-voxel spectroscopy (SVS) techniques were also developed in the 1980s to acquire localized spectra from a 3D cuboid voxel *in vivo* (47-50). In the late 1980s and early 1990s, Bottomley *et al.* for the first time successfully acquired ^{31}P spectra from multiple voxels simultaneously in human brain (51) and heart (52) using spectroscopic imaging approach, opening the door of ^{31}P magnetic resonance spectroscopic imaging (^{31}P-MRSI) to provide unprecedented dimensions of spatial and spectral information in metabolic investigations.

Comparing to non-localized or SVS techniques, imaging acquisition time for ^{31}P-MRSI methods is considerably longer. It has been impractical to perform ^{31}P-MRSI at low-field clinical scanners with adequate resolution and scan time. Preclinical ^{31}P and other hetero-nuclei MRSI studies are commonly performed at high fields for SNR gain (53-55). However, the requirement of high spatial resolution for small animal imaging still renders ^{31}P-MRSI challenging. In recent years, the increased availability of clinical high-field scanners has provided the opportunity to achieve a satisfactory balance between SNR and spatial resolution within the acceptable acquisition time. Further, many promising new techniques have emerged from the development of fast ^{1}H-MRI methods in the past decade. Some of these techniques, such as compressed sensing, non-Cartesian encoding, and the subspace approach, already have shown their potential in accelerating MRSI acquisition. These exciting new developments give rise to renewed interest in ^{31}P and other hetero-nuclei MRSI. It can be expected that more fast MRSI techniques will

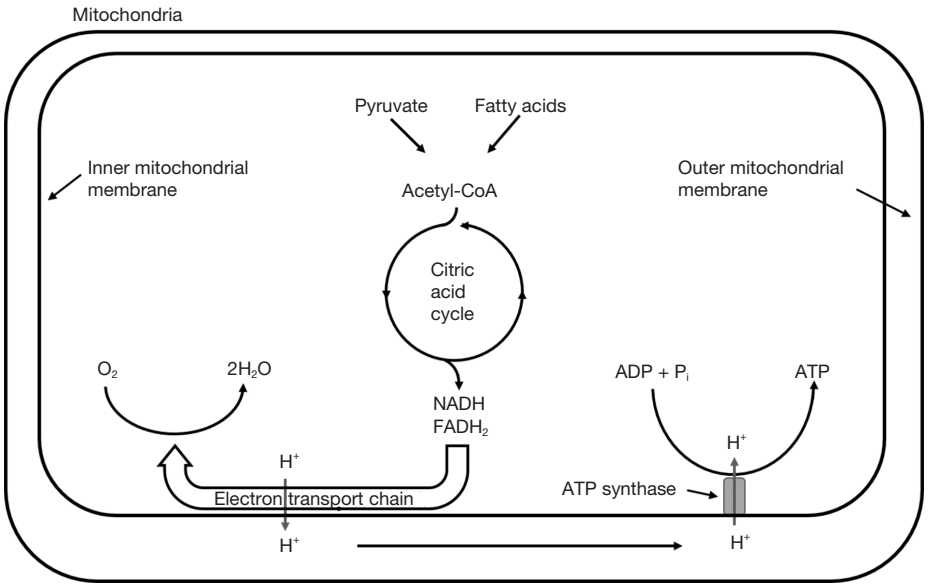

Figure 1 Oxidative phosphorylation in mitochondria. The acetyl group in acetyl-CoA is oxidized through the citric acid cycle, generating electron-rich reducing equivalents NADH and $FADH_2$. The electrons are transferred to oxygen in the electron transport chain, coupled with the pump of protons to the intermembrane space. The proton gradient across the inner mitochondrial membrane is used to drive ATP synthesis via ATP synthase.

emerge that can eventually make metabolic evaluation on clinical patients feasible.

Energy metabolism in living tissues

Under nonischemic conditions, ATP is generated mainly from oxidative phosphorylation in the mitochondria, and to a lesser extent from glycolysis in the cytosol. The oxidation of carbohydrates and fatty acids produces electron-rich molecules, namely the reduced forms of nicotinamide adenine dinucleotide (NADH) and flavin adenine dinucleotide ($FADH_2$). During oxidative phosphorylation, electrons are transferred from NADH and $FADH_2$ to oxygen through a series of redox reactions called the electron transport chain (ETC). The energy released in ETC is used to pump protons (H^+) from mitochondrial matrix to the intermembrane space, which creates an electrochemical proton gradient that drives the synthesis of ATP via ATP synthase. The ATP synthase is a transmembrane protein complex that allows protons in the intermembrane space to flow down its concentration gradient and uses the released energy to synthesize ATP from adenosine diphosphate (ADP) and P_i (*Figure 1*). The stoichiometric links between NADH and $FADH_2$ oxidation, oxygen consumption, and ATP synthesis are described by the following reactions:

$$NADH + H^+ + \frac{1}{2}O_2 + 3ADP + 3P_i \rightarrow NAD^+ + H_2O + 3ATP$$

$$FADH_2 + H^+ + \frac{1}{2}O_2 + 2ADP + 2P_i \rightarrow FADH^+ + H_2O + 2ATP$$

Since ATP is required in many cellular processes including protein synthesis, ion transport, and muscle contraction, the normal rate of ATP hydrolysis is high even at resting state. However, ATP concentration in tissue is relatively low, thus the turnover rate of ATP is also high. Taking heart as an example, ATP hydrolysis rate is typically ~0.5 μmol/g wet wt/s at rest, while ATP concentration is only ~5 μmol/g wet wt. Hence, there is complete turnover of the myocardial ATP pool in every 10 s (56), and this turnover rate is much higher during exercise. In the healthy tissue, the rate of ATP generation is exquisitely linked to the rate of ATP hydrolysis such that ATP content remains constant even with large increase in ATP utilization. This underscores the importance of energy metabolism and its regulation.

Besides oxidative phosphorylation, creatine kinase (CK) is also a key player in maintaining cellular energy homeostasis in many metabolically demanding tissues including muscle and brain (57). CK uses creatine (Cr) for reversible phosphoryl transfer between ATP and PCr in the

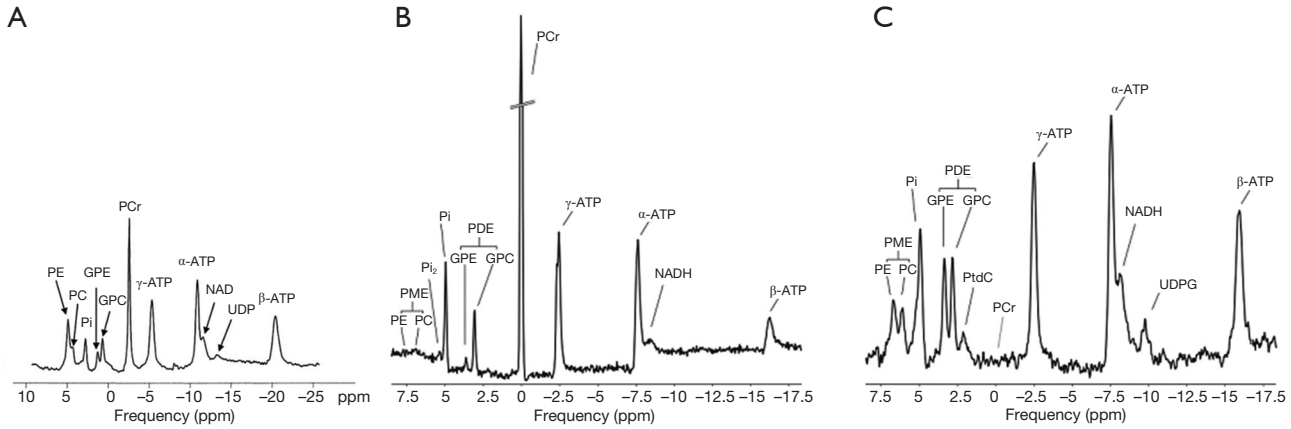

Figure 2 Representative ^{31}P spectra from human brain (A), skeletal muscle (B), and liver (C). Reproduced with permission from Lei *et al*. (67) and from Valkovič (11).

following reaction:

$$ADP + PCr + H^{+} \; f \; ATP + Cr$$

During periods of increased energy demand (e.g., exercise or muscle stimulation) or reduced mitochondrial ATP generation (e.g., ischemia or hypoxia), CK allows rapid transfer of the high-energy phosphate group in PCr to ADP through its forward reaction. As a result, PCr level declines rapidly while ATP reduction is minimal at the early onset of heavy exercise or severe ischemia. Hence, PCr is considered an energy reservoir that is important for maintaining a constant level of ATP during these physiological or pathological perturbations. Upon the end of the perturbation, the PCr pool is replenished by ATP generated through oxidative phosphorylation via the reverse CK reaction. The rate of PCr recovery is considered an indicator of mitochondrial oxidative capacity and thus provides a way to evaluate mitochondrial function *in vivo* by ^{31}P-MRS/MRI (58-62).

Metabolic assessment by ^{31}P-MRS/MRI

Comparing to imaging protons in water, ^{31}P-MRS/MRI is challenged by the low MR sensitivity and low concentrations of phosphate metabolites. In human skeletal muscle, the concentrations of PCr, ATP, and P_i are approximately 30, 10, and 5 mM, respectively (63), which are four orders of magnitude lower than water protons in tissue. On the other hand, the Larmor frequency of ^{31}P is 2.5 times lower and its MR sensitivity is 15 times lower than that of proton (64). However, ^{31}P also has some unique properties that make it advantageous to perform ^{31}P-MRS/MRI. First, ^{31}P has a natural abundance of 100%; hence, it is relatively easy to detect ^{31}P nuclei compared to other MR-detectable nuclei such as carbon-13 and oxygen-17. Second, there are only a few resonance peaks dispersed in a wide range of about 30 ppm in a ^{31}P spectrum, resulting in more straightforward peak quantification. Third, unlike ^{1}H-MRS/MRI, no suppression techniques are needed in ^{31}P-MRS/MRI due to the absence of dominant water or fat signal. Finally, the T_1 relaxation time of phosphate metabolites decreases significantly at a higher field strength (65,66), which allows data acquisition with a relatively short repetition time (TR).

Determination of metabolite concentrations and tissue pH by ^{31}P-MRS

Figure 2 shows ^{31}P spectra from brain, skeletal muscle, and liver, respectively (68). In brain and skeletal muscle, the dominant signal is from PCr, which is usually assigned a chemical shift of 0 ppm due to its relative stability and prominence. P_i and the phospholipids, including phosphomonoesters (PME) and phosphodiesters (PDE), are located to the left of PCr. Resonant peaks from the three phosphate groups of ATP (γ-, α-, and β-ATP from left to right) are located to the right of PCr. Nicotinamide adenine dinucleotide (NAD) in its oxidized and reduced form, i.e., NAD+ and NADH, can also be detected. The concentration of ADP under physiological conditions is too low to be detected by *in vivo* ^{31}P-MRS. However, ADP

can be calculated indirectly from the concentrations of PCr, ATP, and Cr from the chemical equilibrium of the CK reaction (69,70),

$$C_{ADP} = \frac{[Cr] \times [ATP]}{[PCr] \times [H^+] \times K_{CK}}$$

The equilibrium constant of CK (K_{CK}) is approximately 1.66×10^9 M^{-1} (71). The concentration of Cr can be calculated by assuming that PCr represents ~85% of total Cr (72), which is 42 mM from muscle biopsies (73).

Direct quantification of metabolite concentrations from a ^{31}P spectrum is complicated by several factors such as coil sensitivity, field inhomogeneity, and relaxation time. Frequently, a concentration reference is used to convert relative signal intensity to absolute concentrations. A small phantom with known concentration of P_i placed beside the image object can be used as an external reference (74). However, a correction factor is needed to account for the differences in field strength, coil sensitivity, and T_1 saturation between the external reference and metabolites. The accurate estimation of the correction factor requires the measurements of B_1 field map of the ^{31}P transceiver coil, which is much more time consuming than B_1 mapping in ^1H-MRI. A study on human calf muscle reported >1 hour acquisition time to acquire a B_1 map for a ^{31}P volume coil (75). Hence, the external reference approach is not always practical. ATP has also been used as an internal reference because its concentration is relatively stable (~8.2 mM cell water) (76). However, baseline ATP concentration may change in chronic diseases (77-79), limiting the use of this approach in diseased tissues. Alternatively, many studies have used metabolite concentration ratios such as PCr-to-P_i and PCr-to-ATP ratios to evaluate metabolic changes in a variety of diseased conditions (4,80-88). Reduced PCr-to-ATP ratio has been reported as a consequence of reduced CK activity or a loss of the total Cr content in heart diseases (82,89-91).

Besides metabolite concentrations, ^{31}P-MRS also provides a non-invasive tool to measure tissue pH *in vivo*. The chemical shifts of many phosphorus compounds are pH dependent, because protonation of a compound changes the electron distribution surrounding the nuclei and thus changes their resonance frequencies. In a ^{31}P spectrum, the chemical shift of P_i is most sensitive to changes in pH near neutrality because the dissociation constant (pK) of P_i, i.e., the pK of $H_2PO_4^- \rightleftharpoons H^+ + HPO_4^{2-}$, is approximately 7. Hence, from the observed chemical shift of P_i (δ), which is a concentration-weighted sum of the chemical shifts of $H_2PO_4^-$ ($\delta_{H_2PO_4^-}$) and HPO_4^{2-} ($\delta_{HPO_4^{2-}}$), tissue pH can be calculated as

$$pH = pK + \log\left(\frac{\delta - \delta_{H_2PO_4^-}}{\delta_{HPO_4^{2-}} - \delta}\right)$$

For cardiac and skeletal muscle, pK, $\delta_{H_2PO_4^-}$, and $\delta_{HPO_4^{2-}}$ are 6.75, 3.27, and 5.69, respectively (60). In the brain, these values differ slightly at 6.77, 3.29, and 5.68, respectively (92,93). Because of the low concentration of P_i, it is important to acquire a high SNR spectrum for accurate pH quantification. In the liver, the lack of a PCr peak renders pH quantification by chemical shift difference between P_i and PCr challenging. Alternatively, the chemical shift of α-ATP is relatively insensitive to pH and can also serve as an internal frequency reference (94).

Assessment of mitochondrial oxidative capacity by dynamic ^{31}P-MRS

As stated previously, PCr recovery rate upon the end of a metabolic perturbation can be used as an index of mitochondrial oxidative capacity (95). In skeletal muscle, the perturbation is usually induced by sustained muscle contraction or ischemia. Continuous acquisition of ^{31}P spectra during exercise-recovery or ischemia-reperfusion provides the potential to assess mitochondrial oxidative capacity by quantifying the kinetics of PCr depletion and replenishment. Dynamic ^{31}P-MRS has been applied to assess skeletal muscle bioenergetics under physiological conditions (60,61,87,96-99), as well as to evaluate mitochondrial function in skeletal muscle in both diabetic patients and animal models of diabetes (8,100-102).

Figure 3 shows dynamic ^{31}P spectra and the changes of phosphate metabolites and pH during muscle contraction and recovery in human skeletal muscle (103). Similar response (*Figure 4*) can also be observed in animal models during ischemia and reperfusion (102). At the onset of exercise or ischemia, PCr hydrolysis causes a slight increase in pH initially, however, this is quickly followed by a decrease in pH as a result of lactate accumulation (95). Upon the cessation of exercise or ischemia, PCr, P_i, and pH recover to baseline level.

The time constant of PCr recovery in calf muscle is about 25 to 35 s in humans (99,104) and 50 to 90 s in small animals (96,99,102,105). Prolonged PCr recovery is considered to reflect deficits in mitochondrial oxidative metabolism (6,106). To capture the kinetics of PCr recovery, a temporal resolution of <10 s in humans and <20 s in small animals is desirable. Short TR (~2 s) is frequently used to achieve a high temporal resolution (107). To obtain absolute

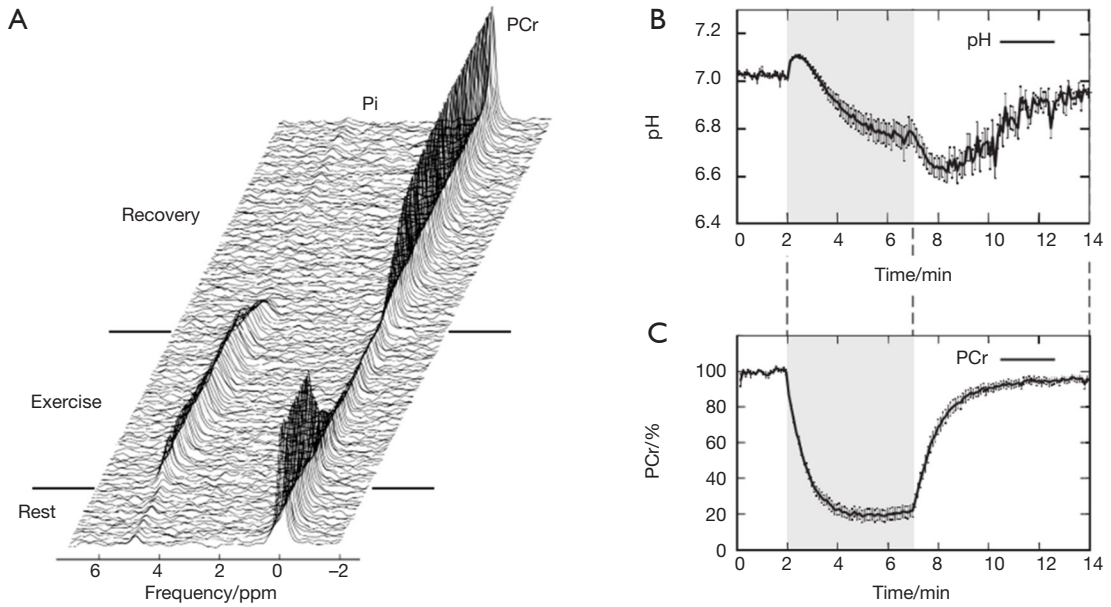

Figure 3 Time series of ^{31}P spectra (A), pH (B), and PCr (C) from human skeletal muscle during exercise and recovery. Reproduced with permission from Schmid *et al.* (103). PCr, phosphocreatine.

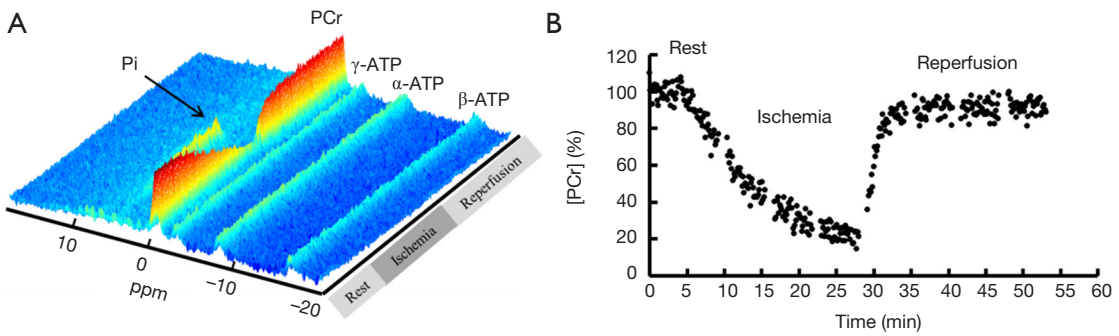

Figure 4 Dynamic ^{31}P spectra (A) and PCr concentration change (B) in rat skeletal muscle at 9.4T during 4-min baseline, 26-min ischemia, and 26-min reperfusion with a temporal resolution of 8 s. PCr, phosphocreatine.

quantification of the metabolites, a fully relaxed spectrum using long TR is usually acquired at resting state to correct for T_1 saturation.

Quantification of ATP synthesis rates by 31P magnetization-transfer MRS

Magnetization transfer (MT) allows for quantification of chemical exchange rates at equilibrium conditions. MT was first developed by Forsen and Hoffmann in the 1960s to study the chemical exchange of protons (108). Brown and Ogawa were the first to measure the unidirectional rates of catalyzed exchanges in an *in vitro* adenylate kinase system using ^{31}P MT-MRS technique (109). Later, similar techniques were applied to the measurements of the ATPase reaction in suspension of aerobic *Escherichia coli* cells (110) and the CK reaction in perfused rat hearts (111). *In vivo* fluxes between PCr and ATP in rat brain and skeletal muscle were quantified using MT in the 1980s (112). Since then, this technique has been widely applied to measure CK reaction rate in heart, brain, and skeletal muscle (17,73,112-117). P_i-to-ATP flux has also been investigated in liver, heart,

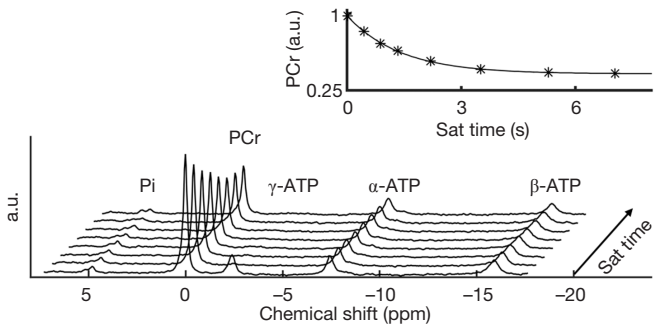

Figure 5 Quantification of the CK reaction rate by ^{31}P MT-MRS. The saturation of γ-ATP induces a reduction in PCr signals via the CK reaction. PCr signal reduction as a function of saturation time follows an exponential relationship. Reproduced with permission from Wang *et al*. (124). PCr, phosphocreatine.

brain, and skeletal muscle (17,118-121). Metabolic abnormalities associated with various diseases including diabetes (17,120), heart failure (7), and stroke (122) have also been evaluated using this technique.

The MT technique is based on the principle that perturbation of the MR signal from an exchanging species (A) can be detected in the MR signal of its exchange partner (B), provided that the T_1 relaxation time of B is comparable to or longer than the lifetime of A. Signal changes in B induced by the exchange of the perturbed nuclei was incorporated into the modified Bloch equation by McConnell (123), which allowed the quantification of the exchange rate by MT methods. In ^{31}P-MRS, the technique enables *in vivo* measurements of metabolic fluxes by perturbing the signal from a specific metabolite (e.g., ATP) and monitoring how the perturbation is transferred to another metabolite (e.g., P_i or PCr) that is linked by an exchange reaction (e.g., ATP synthase or CK). The perturbation can be in the form of either saturation or inversion, which is achieved by applying a frequency-selective saturation or inversion pulse prior to data acquisition.

A typical MT-MRS acquisition involves three steps: the perturbation, or "tagging", of the nuclei of one exchanging species, the transfer of the "tagged" nuclei to the exchange partner, and the measurement of "tag" accumulation in the exchange partner, which reflects the exchange rate. In a typical ^{31}P MT-MRS experiment using saturation transfer (ST), the saturation of γ-ATP induces a signal decrease in both PCr and P_i, with the signal reduction as a function of saturation time follows an exponential relationship (*Figure 5*). The time constant, called the apparent T_1 (T_{1app}), is related to T_1 relaxation time and the forward exchange rate (k_f) by

$$\frac{1}{T_{1app}} = \frac{1}{T_1} + k_f$$

when signal reduction from MT and signal recovery from T_1 relaxation reaches equilibrium, the magnetization reaches its steady-state value (M*), which is related to the equilibrium magnetization (M_0) by

$$M^* = \frac{M_0}{1 + k_f \cdot T_1}$$

Hence, the forward exchange rate can be determined by fitting these equations to experimental data acquired with varied saturation time. Since each acquisition is followed by a long waiting period to reestablish the equilibrium conditions, acquisition time of an MT experiment is typically very long, with waiting time amounts to >90% of the total acquisition time. Further, due to the relatively small signal change in P_i (~20%), quantification of ATP synthesis rate via ATP synthase has been quite limited (17).

Most *in vivo* ^{31}P MT-MRS studies have used ST techniques. The relatively simple formalism and the robustness to experimental imperfections of ST methods are attractive for *in vivo* studies. However, the use of long saturation pulses may not always be practical on clinical scanners. Further, the underlying mechanisms of some ST effects are still being debated (12,17,125,126). Several studies have used inversion transfer (IT) to quantify exchange kinetics (127-129). IT does not require long saturation pulses and is less susceptible to unintended MT effects from small pools of metabolites. Another advantage of IT is that the sensitivity to ATP synthesis rate can be enhanced by inverting PCr and all ATP resonances (130). Such an approach can significantly delay the recovery

of γ-ATP, resulting in amplified MT effects between γ-ATP and P_i. However, more comprehensive modelling is necessary to fully account for multiple magnetization exchanges that involve γ-ATP, including the cross-relaxation between γ-ATP and β-ATP, i.e., the nuclear Overhauser effect (NOE) (129).

Several methods have been proposed to accelerate ^{31}P MT-MRS by using a combination of two acquisition strategies. The first strategy uses a reduced number of spectra acquired under partially relaxed conditions, such as in the Four Angle Saturation Transfer (FAST) method (131) and the Triple Repetition Time Saturation Transfer (TRiST) method (132). In FAST, only four spectra are acquired with a short TR (~1 s) and two different flip angles. This strategy allowed the quantification of CK rate constant in human calf muscle at 1.5 T in 3 min whereas conventional MT methods would require over 21 min of acquisition time to achieve similar accuracy (131). In TRiST, two spectra with different TRs are acquired to derive T_{1app}, with the third control spectrum used for estimating steady-state magnetization. The second strategy further reduces the number of acquired spectra by assuming an intrinsic T_1 values. These methods include the Two Repetition Time Saturation Transfer (TwiST) method (133) and the T_1 Nominal method (134). With the rate constant being the only parameter to be determined, only two spectra are acquired. These methods have been adopted to assess high-energy metabolism in human brain (135), heart (136), and skeletal muscle (137).

Recent development of magnetic resonance fingerprinting (MRF) has opened new doors for MT-MRS. MRF extracts multiple parameter maps from signals generated using non-steady-state pulse sequences in conjunction with Bloch simulations and pattern matching (138,139). This parameter estimation framework allows for greater flexibility in pulse sequence design. More importantly, MRF has demonstrated itself to have the highest SNR efficiency in simultaneous mapping of several parameters. Given the multi-parameter nature of ^{31}P MT-MRS measurements, and the similarity in measuring T_1 and the exchange-rate modulated T_{1app} constant in an MT-MRS experiment, an MRF-based MT-MRS method may overcome the low sensitivity and long acquisition time of the conventional ^{31}P MT-MRS methods. In a recent study, Wang *et al.* developed an MRF-based acquisition strategy for quantification of CK activity (CK-MRF) in rat skeletal muscle (124). Their results showed significantly improved measurement reproducibility in 20-s data acquisition, demonstrating the potential of this new MT encoding strategy. The MRF method developed in this study used spectrally selective excitation to acquire signals from PCr and γ-ATP separately. While this approach allows spatial encoding using imaging methods rather than the more time-consuming MRSI methods, it has the limitation of quantifying CK rate only. An MRF-based spectroscopic method that can accurately quantify both CK and ATP synthase activities with high efficiency remains to be expected.

^{31}P-MRS with spatial localization and metabolic mapping by ^{31}P-MRSI

Due to the low SNR nature of ^{31}P-MRS, many early studies used SVS techniques to acquire spectra from a 3D cuboid volume. The development of SVS techniques provides the opportunity for *in vivo* assessment of tissue metabolism from a volume of interest that is not limited to the body surface. However, whether the selected voxel is representative of the tissue or a specific pathology can be questionable. This can be especially problematic in delineating a focal lesion, in which a misplaced voxel will not be of diagnostic values. Further, the limited spatial information provided by a large spectroscopic voxel cannot adequately capture the metabolic heterogeneity in the tissue. MRSI methods, including spectrally selective imaging methods, were developed to enable metabolic mapping in the tissue.

Single voxel ^{31}P-MRS

The selection of a 3D cuboid voxel can be achieved using either single- or multi-acquisition approaches. The single-acquisition techniques include the Point RESolved Spectroscopy (PRESS) and the STimulated Echo Acquisition Mode (STEAM) methods (47-49). The PRESS technique uses sequential 90°-180°-180° RF pulses in the presence of three slice selective gradients in orthogonal planes to acquire the spin-echo from a 3D voxel, while a STEAM sequence uses three 90° RF pulses to acquire a stimulated-echo from a 3D voxel. Although the SNR of a spin-echo is better than that of a stimulated-echo, the long TE resulting from two 180° pulses in a PRESS sequence is not suitable for imaging short T_2 species such as ATP (~25 ms at 7T). In contrast, the second 90° pulse in a STEAM sequence stores the magnetization in the longitudinal direction, leading to a shorter effective TE. However, the SNR of a stimulated-echo is only about half the SNR of a spin echo (140). Because of these limitations, neither PRESS

Table 1 A summary of PCr imaging studies in humans

Reference	Study	Field strength	Organ	Voxel size (mm^3)	Acquisition time
Greenman *et al.* (152)	3D PCr, resting-state	4T	Heart	12.5×12.5×25	9 min 40 s
Greenman *et al.* (151)	2D PCr, resting-state	3T	Skeletal muscle	4.68×4.68×25	4 min
Greenman *et al.* (153)	2D PCr, dynamic	3T	Skeletal muscle	15×15×25	6 s (temporal resolution)
Parasoglou *et al.* (75)	3D PCr, resting-state	3T	Skeletal muscle	4.6×4.6×25	10 min
Parasoglou *et al.* (104)	3D PCr, dynamic	3T&7T	Skeletal muscle	9.2×9.2×50 (3T), 8×8×25 (7T)	24 s (temporal resolution)

nor STAEM are widely used in ^{31}P spectroscopy.

The Image-Selected In vivo Spectroscopy (ISIS) technique is a free induction decay (FID)-based, multi-acquisition technique that provides better SNR (50). In addition, the minimal time delay between spin excitation and signal acquisition is also more favorable for acquiring signals of short T_2 species. Prior to data acquisition, a set of selective inversion pulses and gradients are employed to align longitudinal magnetization in either the positive or the negative directions. The addition and subtraction of the spectra acquired with different sets of gradients allow the signals from the localized voxel to coherently add while those outside the voxel to completely cancel. A 3D ISIS sequence requires a minimum of eight acquisitions. Because spectra are acquired immediately after the excitation pulse, ISIS is a preferred method for detecting short T_2 metabolites and is a more popular method for ^{31}P-MRS (141-146). A voxel size of ~75 mL in human liver has been reported at 7T (145). On the preclinical scanner, a voxel size of 200 to 300 μL has been achieved in mouse heart at 9.4T (144). However, a major limitation of ISIS is its susceptibility to motion artifacts because of the multiple acquisition scheme.

Spectrally selective imaging methods

Spectrally selective imaging methods were developed to provide spatial mapping of a single phosphate metabolite without the prohibitively long acquisition time required by MRSI. Since changes in PCr and P_i during a perturbation protocol are closely associated with mitochondrial function, these two metabolites are frequently the focus of spectrally selective ^{31}P imaging studies.

To select the metabolite of interest (e.g., PCr) for imaging, a frequency-selective excitation pulse can be used without the presence of a slice-selective gradient (147,148). The subsequent image acquisition using phase- and frequency-encoding gradients is similar to that of ^{1}H imaging. The implementation of this approach is relatively straightforward; however, the duration of the RF pulse needs to be sufficiently long to minimize the spillover effects. It is important that the B_0 field within the sensitive volume of the coil is relatively homogeneous such that the resonance frequency of the metabolite is within the bandwidth of the RF pulse. Because of the relatively long T_2 relaxation time of P_i and PCr (180 and 420 ms for P_i and PCr, respectively at 4.7T) (149), signal readout can use fast spin-echo methods such as the rapid acquisition with relaxation enhancement (RARE). An additional advantage of the RARE method is that it can further suppress the signal from unwanted metabolites (150,151). This is accomplished by selecting the time delay between the excitation pulse and the first refocusing pulse to generate a phase shift of $\pi/2$ between the desired (on-resonance) and the unwanted (off-resonance) species at the time when the refocusing pulse is applied, resulting in rapid dephasing of the signal from the unwanted metabolites.

A summary of the human studies using PCr imaging techniques is listed in *Table 1*. Shown in *Figure 6* are maps of PCr distribution in human calf muscle acquired at 3T using spectrally selective 3D turbo spin-echo (TSE) method (75). In addition to PCr, maps of P_i (154) and PCr-to-ATP ratio (155) can also be acquired. An interleaved excitation scheme further enables simultaneous quantification of PCr and P_i, which allows the quantification of pH from the phase difference between PCr and P_i (156). Furthermore, MT has also been incorporated into this approach to allow the mapping of the CK reaction rate (147,148). Comparing to conventional MRSI methods, imaging techniques using spectrally selective approaches provide the opportunity for improved spatial resolution with reduced imaging time, which enables dynamic metabolic mapping during a perturbation protocol. However, the voxel size is still an order of magnitude larger than that of ^{1}H-MRI, even at

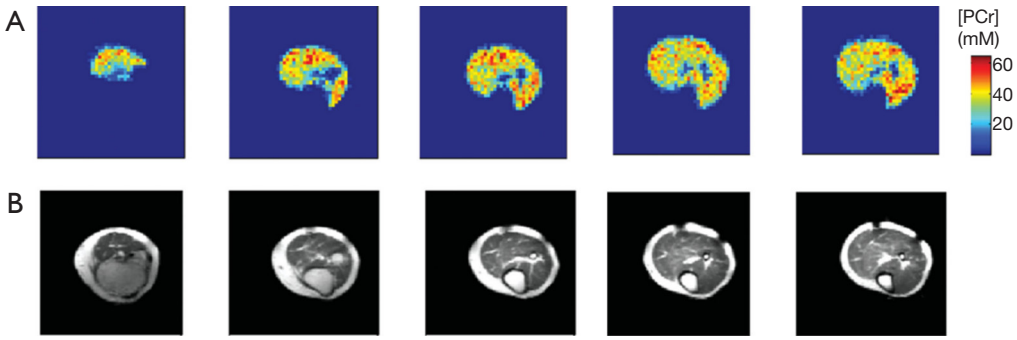

Figure 6 Representative PCr concentration maps of healthy human calf muscle (A) and corresponding ^{1}H anatomical slices (B) acquired using spectrally selective 3D TSE imaging method. Reproduced with permission from Parasoglou *et al*. (75). TSE, turbo spin-echo.

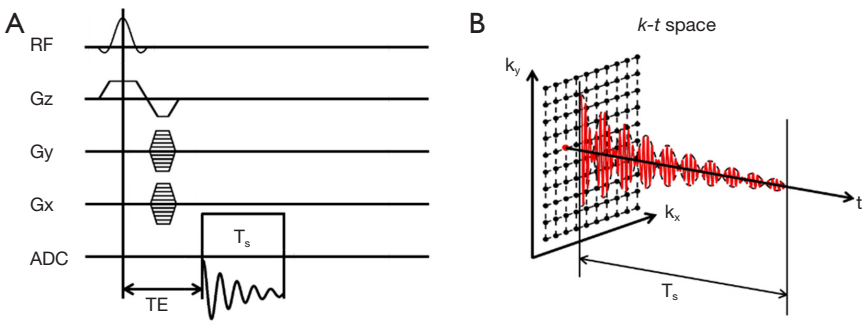

Figure 7 Schematics of a 2D MRSI pulse sequence (A) and the corresponding k-t space filling (B). T_s, acquisition time of a single FID.

high-field scanners. Hence, these techniques have not been applied to preclinical studies because of the requirement of much higher spatial resolution for imaging small animals.

31P-MRSI methods

MRSI, also known as chemical shift imaging (CSI), combines conventional MRI and spectroscopic methods to enable the acquisitions of spectra from multiple voxels simultaneously. MRSI using Fourier-transform approach was proposed in the early 1980s (157,158). In a classical MRSI sequence, the FID signal is acquired without a frequency-encoding gradient such that the readout can be used for chemical-shift encoding. Spatial encoding is achieved using a combination of slice-selective and phase-encoding gradients. Hence, a 2D MRSI sequence samples the k-t space with two orthogonal phase-encoding directions (*Figure* 7). The dwell time of signal sampling determines the spectral bandwidth, while the duration of sampling (T_s) determines the spectral resolution. The additional phase-encoding directions and the need for a large number of signal averages render MRSI acquisition extremely time consuming. As a tradeoff, MRSI data are frequently acquired at low spatial resolution with as few as 8 phase encoding steps in one dimension (159-161).

The small coverage of the k-space with low resolution MRSI gives rise to side-lobes in the spatial response function (SRF), which causes significant cross-voxel contamination and thus poor localization precision. These side-lobes can be reduced by applying a k-space filter that gives more weight to the center of k-space. However, applying the filter in post-processing reduces spatial resolution and SNR efficiency (162). Alternatively, weighted k-space acquisition has been proposed to improve the SRF without sacrificing spatial resolution and SNR efficiency (163-166). This strategy has been used in most of the ^{31}P MRSI studies. Depending on the coil and field strength, k-space weighted ^{31}P-MRSI can typically achieve a voxel size of 18 to 47 mL in liver with an acquisition time of ~30 min (167,168). At 7T, Lei and colleagues were able to acquire 3D ^{31}P-MRSI data from human brain with a voxel size of 7.5 mL in 7.85 min (73). The acquisition time can be

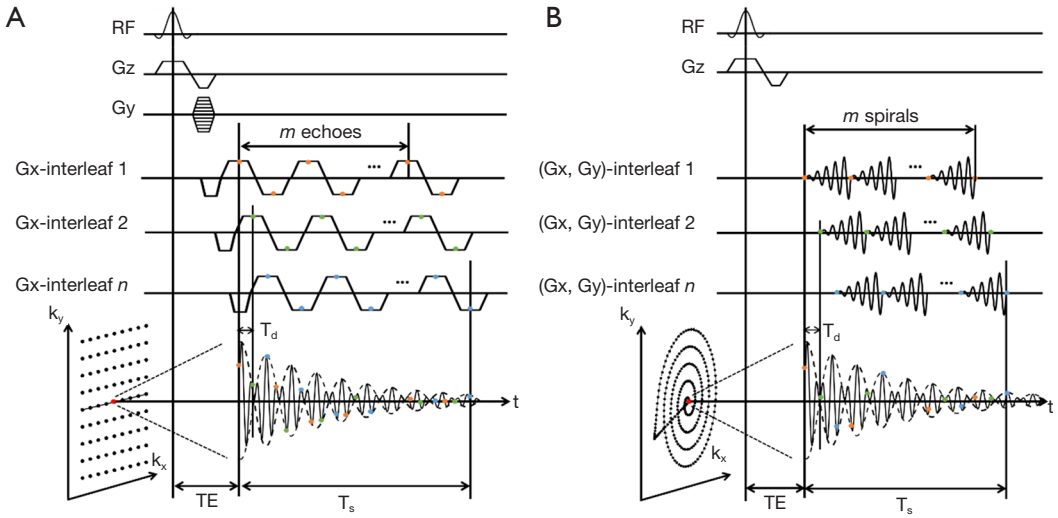

Figure 8 Schematics of 2D EPSI (A) and spiral MRSI (B) sequences. T_s, acquisition time of a single temporal interleaf; T_d, time delay between two consecutive temporal interleaves.

significantly prolonged in cardiac ^{31}P-MRSI studies due to the requirement of triggering (169).

Several approaches to accelerate MRSI acquisition have been proposed. Echo-planar spectroscopic imaging (EPSI) was initially developed for ^{1}H-MRSI (170). The technique uses a rapidly oscillating readout gradient for simultaneous encoding of spectral and spatial information, thus reducing the acquisition time (*Figure 8A*). A major limitation of EPSI is the demand on strong, fast switching gradients with excellent eddy current performance to minimize the ghosting artifacts. The lower gyromagnetic ratio of ^{31}P nuclei requires even higher gradient amplitude and slew rate. An alternative to EPSI is to use non-Cartesian trajectories such as spiral (171) and rosette (172) for simultaneous encoding of spectral and spatial information, with reduced demand on gradient performance (*Figure 8B*). Due to the large spectral dispersion in ^{31}P spectra, both EPSI and non-Cartesian encoding need to use temporal interleaves to increase spectral bandwidth in ^{31}P-MRSI. The spectral bandwidth is therefore inversely proportional to the time delay (T_d) between two consecutive temporal interleaves.

Both EPSI and spiral MRSI have been attempted in ^{31}P-MRSI. The feasibility of using EPSI in mapping ^{31}P metabolites was recently demonstrated by Korzowski and Bachert at 7T, achieving an effective volume of 4.05 mL with less than 12 min acquisition in human calf muscle, and an effective volume of 16.2 mL in less than 10 min in the brain (173). Using spiral acquisition, Valkovič and colleagues were able to acquire dynamic ^{31}P-MRSI during exercise at 7T, albeit with reduced SNR (174). It is important to note that the acceleration achieved by EPSI and non-Cartesian MRSI is accompanied by SNR loss. This is because at the presence of a readout gradient the effective T_2* is reduced while the signal bandwidth is increased. Although more signal averages can be performed with a fixed acquisition time, the SNR efficiency, i.e., $SNR/\sqrt{\text{Acquisition time}}$, is not improved comparing to conventional MRSI method (175).

The excellent SNR efficiency of balanced steady-state free precession (bSSFP) has also been exploited in ^{31}P-MRSI to achieve acceleration. Speck *et al.* developed a bSSFP-based ^{31}P-MRSI technique and demonstrated it in human skeletal muscles at 2T (176). *In vivo* results showed a 4 to 5 fold acceleration with the same SNR compared to fast low angle shot (FLASH)-based MRSI methods. A multi-echo bSSFP MRSI method was applied to ^{1}H and ^{31}P to further reduce the acquisition time (177). However, bSSFP requires short TR to minimize the banding artifact. Given the large dispersion of ^{31}P metabolites (~30 ppm), TR of less than 10 ms still renders multiple null bands in the spectrum. The severe frequency-dependent spectral modulation constrains the flexibility of choosing acquisition parameters to avoid the resonances of interest falling in the null band, limiting the applications of this approach in both preclinical and clinical research (176).

Recently, a subspace based approach, called SPectroscopic Imaging by exploiting spatiospectral CorrElation (SPICE),

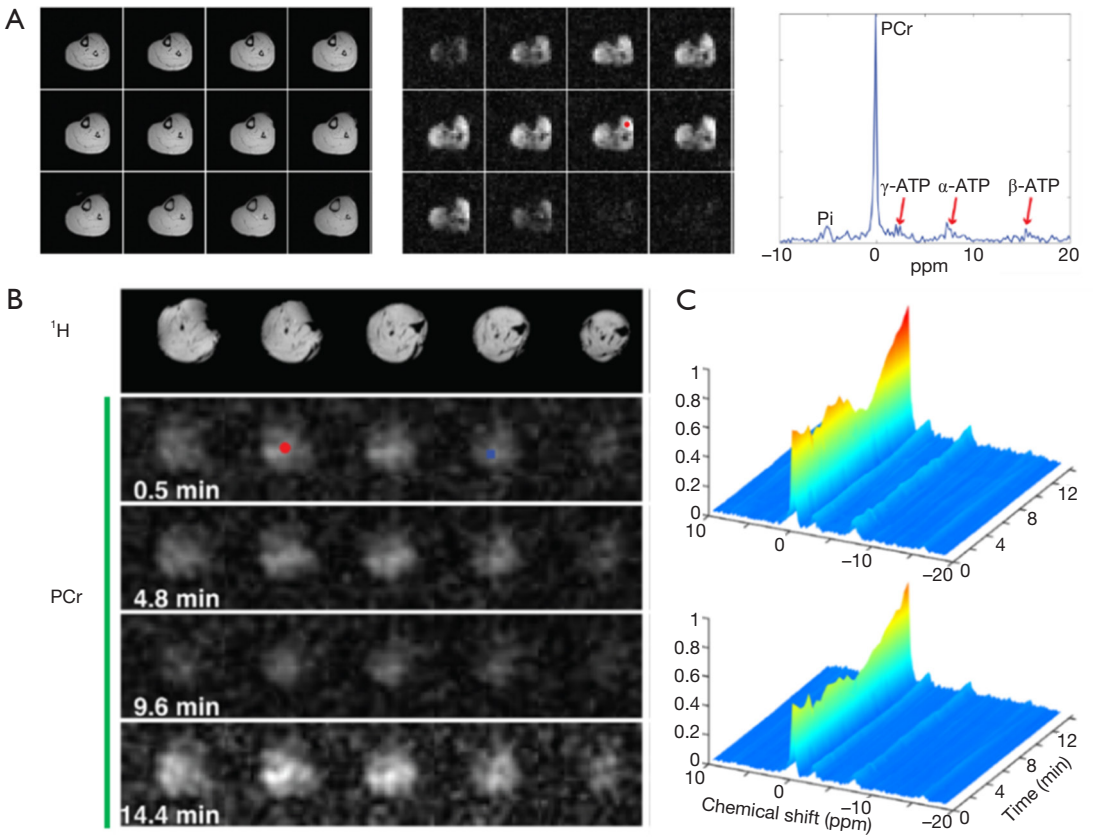

Figure 9 ^{31}P-MRSI using SPICE. (A) ^{1}H images (left), PCr maps (middle), and a ^{31}P spectrum (right) obtained from human calf muscle at 3T. The location of the spectrum is indicated by the red circle in PCr maps. (B) Anatomic ^{1}H images and dynamic PCr images of rat hindlimb during ischemia/reperfusion obtained at 9.4T. (C) Dynamic spectra from two different spatial locations corresponding to the red circle (upper) and blue square (bottom) in (B). Reproduced with the permission from Ma *et al.* (181).

has emerged as a promising technique for high-resolution MRSI (178). The technique takes advantage of a unique property of spectroscopic signals known as the partial separability (PS), which indicates that high-dimensional spectroscopic signals reside in a very low-dimensional subspace. Hence, a low-rank model that captures the spatiospectral correlation of the MRSI data can be used for high-resolution MRSI reconstruction from undersampled data. The potential of SPICE for accelerated data acquisition was initially demonstrated in ^{1}H-MRSI, achieving 3D MRSI at 3 mm isotropic resolution in less than 10-min acquisition (179,180). Comparing to a ^{1}H spectrum, a ^{31}P spectrum contains fewer resonance peaks with large chemical shift dispersion. In addition, ^{31}P spectra are not contaminated or distorted by signals from water and lipids. These unique properties make the application of SPICE to ^{31}P-MRSI particularly promising because the rank of the model can be further reduced, allowing greater potential for undersampling and acceleration. Indeed, a recent dynamic ^{31}P-MRSI study by Ma *et al.* achieved unprecedented spatial and temporal resolutions in both human subjects and laboratory animals (181). On a 3T whole-body scanner, ^{31}P-MRSI of human calf muscle with a nominal spatial resolution of 6.9×6.9×10 mm^3 (0.47 mL) was achieved within 15 min acquisition (*Figure 9A*). On a 9.4T preclinical scanner, dynamic ^{31}P-MRSI data were acquired from rat hindlimb with high spatial (1.5×1.5×1.6 mm^3) and temporal (30 s) resolution (*Figure 9B,C*). These preliminary results demonstrate the potential of this approach to quantify metabolic heterogeneity in both patients and small animals.

Besides the fast MRSI methods described above, other fast imaging strategies commonly used in ^{1}H-MRI such as parallel imaging (182-184) and compressed sensing (185) are also promising to be combined with MRSI techniques

to further accelerate the acquisition. These techniques have already been applied to imaging hyperpolarized carbon-13 molecules (186,187). Compressed sensing has also been combined with spectrally selective ^{31}P imaging to accelerate the imaging of PCr recovery kinetics in humans (188). With renewed interest in metabolic imaging, more translations of these promising techniques to ^{31}P-MRSI will emerge in the near future.

Conclusions

^{31}P-MRS/MRI/MRSI provides a powerful and versatile tool to probe energy metabolism *in vivo*. The development of advanced hardware system and novel acquisition/reconstruction strategies in recent years brings enormous opportunities to ^{31}P-MRS/I techniques to extend its application in both clinical and preclinical studies with improved sensitivity and efficiency. Improved ^{31}P-MRS/I techniques will further enhance our understanding of underlying mechanisms of bioenergetics and physiological and pathological influences on energy metabolism in various organs and tissue types.

Acknowledgements

Funding: This work is supported by grants from U.S. National Institute of Health (R21 HL126215 and R01 EB23704).

Footnote

Conflicts of Interest: The authors have no conflicts of interest to declare.

References

1. Neubauer S. The failing heart--an engine out of fuel. N Engl J Med 2007;356:1140-51.
2. DeBerardinis RJ, Thompson CB. Cellular Metabolism and Disease: What Do Metabolic Outliers Teach Us? Cell 2012;148:1132-44.
3. Neeman M, Rushkin E, Kaye AM, Degani H. 31P-NMR studies of phosphate transfer rates in T47D human breast cancer cells. Biochim Biophys Acta 1987;930:179-92.
4. Bottomley PA, Drayer BP, Smith LS. Chronic adult cerebral infarction studied by phosphorus NMR spectroscopy. Radiology 1986;160:763-6.
5. Levine SR, Helpern JA, Welch KM, Vande Linde AM, Sawaya KL, Brown EE, Ramadan NM, Deveshwar RK, Ordidge RJ. Human focal cerebral ischemia: evaluation of brain pH and energy metabolism with P-31 NMR spectroscopy. Radiology 1992;185:537-44.
6. Scheuermann-Freestone M, Madsen PL, Manners D, Blamire AM, Buckingham RE, Styles P, Radda GK, Neubauer S, Clarke K. Abnormal cardiac and skeletal muscle energy metabolism in patients with type 2 diabetes. Circulation 2003;107:3040-6.
7. Weiss RG, Gerstenblith G, Bottomley PA. ATP flux through creatine kinase in the normal, stressed, and failing human heart. Proc Natl Acad Sci USA 2005;102:808-13.
8. Befroy DE, Petersen KF, Dufour S, Mason GF, de Graaf RA, Rothman DL, Shulman GI. Impaired mitochondrial substrate oxidation in muscle of insulin-resistant offspring of type 2 diabetic patients. Diabetes 2007;56:1376-81.
9. Lu M, Chen W, Zhu X. Field dependence study of in vivo brain (31) P MRS up to 16.4 T. NMR Biomed 2014;27:1135-41.
10. Campbell MD, Marcinek DJ. Evaluation of in vivo mitochondrial bioenergetics in skeletal muscle using NMR and optical methods. Biochim Biophys Acta 2016;1862:716-24.
11. Valkovič L, Chmelík M, Krššák M. In-vivo 31P-MRS of skeletal muscle and liver: A way for non-invasive assessment of their metabolism. Anal Biochem 2017;529:193-215.
12. Kemp GJ, Brindle KM. What do magnetic resonance-based measurements of Pi→ATP flux tell us about skeletal muscle metabolism? Diabetes 2012;61:1927-34.
13. Holloway CJ, Suttie J, Dass S, Neubauer S. Clinical Cardiac Magnetic Resonance Spectroscopy. Prog Cardiovasc Dis 2011;54:320-7.
14. Bainbridge A, Tachtsidis I, Faulkner SD, Price D, Zhu T, Baer E, Broad KD, Thomas DL, Cady EB, Robertson NJ, Golay X. Brain mitochondrial oxidative metabolism during and after cerebral hypoxia-ischemia studied by simultaneous phosphorus magnetic-resonance and broadband near-infrared spectroscopy. Neuroimage 2014;102:173-83.
15. Abdel Razek AA, Poptani H. MR spectrsocopy of head and neck cancer. Eur J Radiol 2013;82:982-9.
16. Holloway C, ten Hove M, Clarke K, Neubauer S. MR spectroscopy in heart failure. Front Biosci (Schol. Ed) 2011;3:331-40.
17. Befroy DE, Rothman DL, Petersen KF, Shulman GI. 31P-magnetization transfer magnetic resonance spectroscopy measurements of in vivo metabolism.

Diabetes 2012;61:2669-78.
18. Hwang JH, Choi CS. Use of in vivo magnetic resonance spectroscopy for studying metabolic diseases. Exp Mol Med 2015;47:e139.
19. Cohn M, Hughes TR Jr. Phosphorus magnetic resonance spectra of adenosine di- and triphosphate. I. Effect of pH. J Biol Chem 1960;235:3250-3.
20. Lauterbur PC. Image formation by induced local interactions. Examples employing nuclear magnetic resonance. 1973. Clin Orthop Relat Res 1989;(244):3-6.
21. Moon RB, Richards JH. Determination of intracellular pH by 31P magnetic resonance. J Biol Chem 1973;248:7276-8.
22. Henderson TO, Costello AJ, Omachi A. Phosphate metabolism in intact human erythrocytes: determination by phosphorus-31 nuclear magnetic resonance spectroscopy. Proc Natl Acad Sci USA 1974;71:2487–90.
23. Hoult DI, Busby SJW, Gadian DG, Radda GK, Richards RE, Seeley PJ. Observation of tissue metabolites using 31P nuclear magnetic resonance. Nature 1974;252:285-7.
24. Chance B, Nakase Y, Bond M, Leigh JS, McDonald G. Detection of 31P nuclear magnetic resonance signals in brain by in vivo and freeze-trapped assays. Proc Natl Acad Sci U S A 1978;75:4925-9.
25. Ogawa S, Rottenberg H, Brown TR, Shulman RG, Castillo CL, Glynn P. High-resolution 31P nuclear magnetic resonance study of rat liver mitochondria. Proc Natl Acad Sci U S A 1978;75:1796-800.
26. Jacobus WE, Lehninger AL. Creatine kinase of rat heart mitochondria. Coupling of creatine phosphorylation to electron transport. J Biol Chem 1973;248:4803-10.
27. Pollard HB, Shindo H, Creutz CE, Pazoles CJ, Cohen JS. Internal pH and state of ATP in adrenergic chromaffin granules determined by 31P nuclear magnetic resonance spectroscopy. J Biol Chem 1979;254:1170-7.
28. Navon G, Ogawa S, Shulman RG, Yamane T. High-resolution 31P nuclear magnetic resonance studies of metabolism in aerobic Escherichia coli cells. Proc Natl Acad Sci U S A 1977;74:888-91.
29. Salhany JM, Yamane T, Shulman RG, Ogawa S. High resolution 31P nuclear magnetic resonance studies of intact yeast cells. Proc Natl Acad Sci U S A 1975;72:4966-70.
30. Cohen SM, Ogawa S, Rottenberg H, Glynn P, Yamane T, Brown TR, Shulman RG. 31P nuclear magnetic resonance studies of isolated rat liver cells. Nature 1978;273:554-6.
31. Burt CT, Glonek T, Bárány M. Analysis of phosphate metabolites, the intracellular pH, and the state of adenosine triphosphate in intact muscle by phosphorus nuclear magnetic resonance. J Biol Chem 1976;251:2584-91.
32. Dawson MJ, Gadian DG, Wilkie DR. Muscular fatigue investigated by phosphorus nuclear magnetic resonance. Nature 1978;274:861-6.
33. Jacobus WE, Taylor GJ, Hollis DP, Nunnally RL. Phosphorus nuclear magnetic resonance of perfused working rat hearts. Nature 1977;265:756-8.
34. Garlick PB, Radda GK, Seeley PJ. Phosphorus NMR studies on perfused heart. Biochem Biophys Res Commun 1977;74:1256-62.
35. Salhany JM, Pieper GM, Wu S, Todd GL, Clayton FC, Eliot RS. 31P Nuclear magnetic resonance measurement of cardiac pH in perfused guinea-pig hearts. J Mol Cell Cardiol 1979;11:601-10.
36. Norwood WI, Norwood CR, Ingwall JS, Castaneda AR, Fossel ET. Hypothermic circulatory arrest: 31-phosphorus nuclear magnetic resonsance of isolated perfused neonatal rat brain. J Thorac Cardiovasc Surg 1979;78:823-30.
37. Sehr PA, Bore PJ, Papatheofanis J, Radda GK. Non-destructive measurement of metabolites and tissue pH in the kidney by 31P nuclear magnetic resonance. Br J Exp Pathol 1979;60:632-41.
38. Canioni P, Desmoulin F, Galons JP, Bernard M, Fontanarava E, Cozzone PJ. Carbon-13 and phosphorus-31 NMR study of hepatic metabolism in the perfused rat liver. Arch Int Physiol Biochim 1985;93:119-28.
39. Salhany JM, Stohs SJ, Reinke LA, Pieper GM, Hassing JM. 31P nuclear magnetic resonance of metabolic changes associated with cyanide intoxication in the perfused rat liver. Biochem Biophys Res Commun 1979;86:1077-83.
40. Ackerman JJ, Grove TH, Wong GG, Gadian DG, Radda GK. Mapping of metabolites in whole animals by 31P NMR using surface coils. Nature 1980;283:167-70.
41. Bendel P, Lai CM, Lauterbur PC. P-31 Spectroscopic Zeugmatography of Phosphorous Metabolites. J Magn Reson (San Diego, Calif 1997) 1980;38:343-56.
42. Bottomley PA, Foster TB, Darrow RD. Depth-resolved surface-coil spectroscopy (DRESS) for in Vivo 1H, 31P, and 13C NMR. J Magn Reson 1984;59:338-42.
43. Bottomley PA. Noninvasive study of high-energy phosphate metabolism in human heart by depth-resolved 31P NMR spectroscopy. Science 1985;229:769-72.
44. Mitsunami K, Okada M, Inoue T, Hachisuka M, Kinoshita M, Inubushi T. In vivo 31P nuclear magnetic resonance spectroscopy in patients with old myocardial infarction.

Jpn Circ J 1992;56:614-9.
45. Bottomley PA, Herfkens RJ, Smith LS, Bashore TM. Altered phosphate metabolism in myocardial infarction: P-31 MR spectroscopy. Radiology 1987;165:703-7.
46. Valkovič L, Chmelík M, Just Kukurová I, Jakubová M, Kipfelsberger MC, Krumpolec P, Tušek Jelenc M, Bogner W, Meyerspeer M, Ukropec J, Frollo I, Ukropcová B, Trattnig S, Krššák M. Depth-resolved surface coil MRS (DRESS)-localized dynamic (31) P-MRS of the exercising human gastrocnemius muscle at 7 T. NMR Biomed 2014;27:1346-52.
47. Bottomley P. Selective volume method for performing localized NMR spectroscopy. Magn Reson Imaging 1985;3:iv-v.
48. Bottomley PA. Spatial localization in NMR spectroscopy in vivo. Ann N Y Acad Sci 1987;508:333-48.
49. Frahm J, Merboldt KD, Hänicke W. Localized proton spectroscopy using stimulated echoes. J Magn Reson 1987;72:502-8.
50. Ordidge R, Connelly A, Lohman J. Image-selected in vovo spectroscopy (ISIS) a new technique for spatially selective NMR spectroscopy. J Magn Reson 1986;66:283-94.
51. Bottomley PA, Charles HC, Roemer PB, Flamig D, Engeseth H, Edelstein WA, Mueller OM. Human in vivo phosphate metabolite imaging with 31P NMR. Magn Reson Med 1988;7:319-36.
52. Bottomley PA, Hardy CJ, Roemer PB. Phosphate metabolite imaging and concentration measurements in human heart by nuclear magnetic resonance. Magn Reson Med 1990;14:425-34.
53. Flögel U, Jacoby C, Gödecke A, Schrader J. In vivo 2D mapping of impaired murine cardiac energetics in NO-induced heart failure. Magn Reson Med 2007;57:50-8.
54. Nahrendorf M, Hiller KH, Greiser A, Kohler S, Neuberger T, Hu K, Waller C, Albrecht M, Neubauer S, Haase A, Ertl G, Bauer WR. Chronic coronary artery stenosis induces impaired function of remote myocardium: MRI and spectroscopy study in rat. Am J Physiol Heart Circ Physiol 2003;285:H2712-21.
55. Cui W, Zhu XH, Vollmers ML, Colonna ET, Adriany G, Tramm B, Dubinsky JM, Oz G. Non-invasive measurement of cerebral oxygen metabolism in the mouse brain by ultra-high field (17)O MR spectroscopy. J Cereb Blood Flow Metab 2013;33:1846-9.
56. Stanley WC, Recchia FA, Lopaschuk GD. Myocardial substrate metabolism in the normal and failing heart. Physiol Rev 2005;85:1093-129.
57. Schlattner U, Klaus A, Ramirez Rios S, Guzun R, Kay L, Tokarska-Schlattner M. Cellular compartmentation of energy metabolism: creatine kinase microcompartments and recruitment of B-type creatine kinase to specific subcellular sites. Amino Acids 2016;48:1751-74.
58. Meyer RA. A linear model of muscle respiration explains monoexponential phosphocreatine changes. Am J Physiol 1988;254:C548-53.
59. Challiss RA, Vranic M, Radda GK. Bioenergetic changes during contraction in diabetic rat skeletal muscle and recovery. Am J Physiol 1989;256:E129-37.
60. Soussi B, Idström JP, Bylund-Fellenius a C, Scherstén T. Dynamics of skeletal muscle energetics during ischemia and reperfusion assessed by in vivo 31P NMR. NMR Biomed 1990;3:71-7.
61. Morikawa S, Kido C, Inubushi T. Observation of rat hind limb skeletal muscle during arterial occlusion and reperfusion by 31P MRS and 1H MRI. Magn. Reson Imaging 1991;9:269-74.
62. Paganini AT, Foley JM, Meyer RA. Linear dependence of muscle phosphocreatine kinetics on oxidative capacity. Am J Physiol 1997;272:C501-10.
63. Kemp GJ, Meyerspeer M, Moser E. Absolute quantification of phosphorus metabolite concentrations in human muscle in vivo by 31P MRS: a quantitative review. NMR Biomed 2007;20:555-65.
64. Zhu XH, Zhang N, Zhang Y, Zhang X, Ugurbil K, Chen W. In vivo 17O NMR approaches for brain study at high field. NMR Biomed 2005;18:83-103.
65. Bogner W, Chmelik M, Schmid AI, Moser E, Trattnig S, Gruber S. Assessment of 31P relaxation times in the human calf muscle: A comparison between 3 T and 7 T in vivo. Magn Reson Med 2009;62:574-82.
66. Qiao H, Zhang X, Zhu XH, Du F, Chen W. In vivo 31P MRS of human brain at high/ultrahigh fields: a quantitative comparison of NMR detection sensitivity and spectral resolution between 4 T and 7 T. Magn Reson Imaging 2006;24:1281-6.
67. de Graaf RA. In Vivo NMR Spectroscopy: Principles and Techniques: 2nd Edition, 2007.
68. Wiseman RW, Kushmerick MJ. Creatine kinase equilibration follows solution thermodynamics in skeletal muscle: 31P NMR studies using creatine analogs. J Biol Chem 1995;270:12428-38.
69. Kemp GJ, Taylor DJ, Thompson CH, Hands LJ, Rajagopalan B, Styles P, Radda GK. Quantitative analysis by 31P magnetic resonance spectroscopy of abnormal mitochondrial oxidation in skeletal muscle during recovery from exercise. NMR Biomed 1993;6:302-10.

70. Harkema SJ, Meyer RA. Effect of acidosis on control of respiration in skeletal muscle. Am J Physiol 1997;272:C491-500.
71. Kemp GJ, Roussel M, Bendahan D, Le Fur Y, Cozzone PJ. Interrelations of ATP synthesis and proton handling in ischaemically exercising human forearm muscle studied by 31P magnetic resonance spectroscopy. J Physiol 2001;535:901-28.
72. Kemp GJ, Meyerspeer M, Moser E, Graham J. Kemp, Martin Meyerspeer EM. Absolute quantification of phosphorus metabolite concentrations in human muscle in vivo by 31P MRS: a quantitative review. NMR Biomed 2007;20:555-65.
73. Lei H, Zhu X, Zhang X, Ugurbil K, Chen W. In vivo 31P magnetic resonance spectroscopy of human brain at 7 T: an initial experience. Magn Reson Med 2003;49:199-205.
74. Roth K, Hubesch B, Meyerhoff DJ, Naruse S, Gober JR, Lawry TJ, Boska MD, Matson GB, Weiner MW. Noninvasive quantitation of phosphorus metabolites in human tissue by NMR spectroscopy. J Magn Reson 1989;81:299-311.
75. Parasoglou P, Xia D, Regatte RR. Spectrally selective 3D TSE imaging of phosphocreatine in the human calf muscle at 3 T. Magn Reson Med 2013;69:812-7.
76. Kemp GJ, Meyerspeer M, Moser E. Absolute quantification of phosphorus metabolite concentrations in human musclein vivo by31P MRS: a quantitative review. NMR Biomed 2007;20:555-65.
77. Oláh J, Klivényi P, Gardián G, Vécsei L, Orosz F, Kovacs GG, Westerhoff HV, Ovádi J. Increased glucose metabolism and ATP level in brain tissue of Huntington's disease transgenic mice. FEBS J 2008;275:4740-55.
78. Moshkova AN, Khvatova EM, Rusakova IA. Analysis and prediction of ATP concentration in the animal brain under hypoxic conditions. Neurochem J 2009;3:44-8.
79. Miot F, van Cauteren M, Rooze AK, Geerts A, Osteaux M, Willem R. Non-Invasive in Vivo Determination of the Absolute ATP Concentration in the Rat Liver by 31P NMR Spectroscopy. Bulletin des Sociétés Chimiques Belges 1992;101:113-8.
80. Weiss RG, Chatham JC, Georgakopolous D, Charron MJ, Wallimann T, Kay L, Walzel B, Wang Y, Kass DA, Gerstenblith G, Chacko VP. An increase in the myocardial PCr/ATP ratio in GLUT4 null mice. FASEB J 2002;16:613-5.
81. Braun KP, Dijkhuizen RM, de Graaf RA, Nicolay K, Vandertop WP, Gooskens RH, Tulleken KA. Cerebral ischemia and white matter edema in experimental hydrocephalus: a combined in vivo MRI and MRS study. Brain Res 1997;757:295-8.
82. Shivu GN, Abozguia K, Phan TT, Ahmed I, Henning A, Frenneaux M. 31P magnetic resonance spectroscopy to measure in vivo cardiac energetics in normal myocardium and hypertrophic cardiomyopathy: Experiences at 3 T. Eur J Radiol 2010;73:255-9.
83. Saggu R. Characterisation of Endothelin-1-Induced Intrastriatal Lesions Within the Juvenile and Adult Rat Brain Using MRI and 31P MRS. Transl Stroke Res 2013;4:351-67.
84. Chanseaume E, Bielicki G, Tardy AL, Renou JP, Freyssenet D, Boirie Y, Morio B. Impaired resting muscle energetics studied by (31)P-NMR in diet-induced obese rats. Obesity (Silver Spring) 2008;16:572-7.
85. Sharma R, Sinha S, Danishad KA, Vikram NK, Gupta A, Ahuja V, Jagannathan NR, Pandey RM, Misra A. Investigation of hepatic gluconeogenesis pathway in non-diabetic Asian Indians with non-alcoholic fatty liver disease using in vivo (31P) phosphorus magnetic resonance spectroscopy. Atherosclerosis 2009;203:291-7.
86. Ten Hove M, Neubauer S. Evaluating metabolic changes in heart disease by magnetic resonance spectroscopy. Heart Metab 2006;32:18-21.
87. Giannesini B, Vilmen C, Le Fur Y, Dalmasso C, Cozzone PJ, Bendahan D. A strictly noninvasive MR setup dedicated to longitudinal studies of mechanical performance, bioenergetics, anatomy, and muscle recruitment in contracting mouse skeletal muscle. Magn Reson Med 2010;64:262-70.
88. Hardy CJ, Weiss RG, Bottomley PA, Gerstenblith G. Altered myocardial high-energy phosphate metabolites in patients with dilated cardiomyopathy. Am Heart J 1991;122:795-801.
89. Ye Y, Gong G, Ochiai K, Liu J, Zhang J. High-energy phosphate metabolism and creatine kinase in failing hearts: a new porcine model. Circulation 2001;103:1570-6.
90. Smith CS, Bottomley PA, Schulman SP, Gerstenblith G, Weiss RG. Altered creatine kinase adenosine triphosphate kinetics in failing hypertrophied human myocardium. Circulation 2006;114:1151-8.
91. Conway MA, Allis J, Ouwerkerk R, Niioka T, Rajagopalan B, Radda GK. Detection of low phosphocreatine to ATP ratio in failing hypertrophied human myocardium by 31P magnetic resonance spectroscopy. Lancet 1991;338:973-6.
92. Petroff OA, Prichard JW, Behar KL, Alger JR, den Hollander JA, Shulman RG. Cerebral intracellular pH by 31P nuclear magnetic resonance spectroscopy. Neurology

1985;35:781-8.
93. Barker PB, Butterworth EJ, Boska MD, Nelson J, Welch KM. Magnesium and pH imaging of the human brain at 3.0 Tesla. Magn Reson Med 1999;41:400-6.
94. Rata M, Giles SL, DeSouza NM, Leach MO, Payne GS. Comparison of three reference methods for the measurement of intracellular pH using 31P MRS in healthy volunteers and patients with lymphoma. NMR Biomed 2014;27:158-62.
95. Befroy DE, Shulman GI. Magnetic resonance spectroscopy studies of human metabolism. Diabetes 2011;60:1361-9.
96. Marro KI, Olive JL, Hyyti OM, Kushmerick MJ. Time-courses of perfusion and phosphocreatine in rat leg during low-level exercise and recovery. J Magn Reson Imaging 2007;25:1021-7.
97. Lanza IR, Bhagra S, Nair KS, Port JD. Measurement of human skeletal muscle oxidative capacity by 31P-MR spectroscopy: A cross-validation with in vitro measurements. J Magn Reson Imaging 2011;34:1143-50.
98. Miller RG, Boska MD, Moussavi RS, Carson PJ, Weiner MW. 31P nuclear magnetic resonance studies of high energy phosphates and pH in human muscle fatigue. Comparison of aerobic and anaerobic exercise. J Clin Invest 1988;81:1190-6.
99. Forbes SC, Paganini AT, Slade JM, Towse TF, Meyer RA. Phosphocreatine recovery kinetics following low- and high-intensity exercise in human triceps surae and rat posterior hindlimb muscles. Am J Physiol Regul Integr Comp Physiol 2009;296:R161-70.
100. Perry CG, Kane DA, Lanza IR, Neufer PD. Methods for assessing mitochondrial function in diabetes. Diabetes 2013;62:1041-53.
101. Macia M, Pecchi E, Vilmen C, Desrois M, Lan C, Portha B, Bernard M, Bendahan D, Giannesini B. Insulin Resistance Is Not Associated with an Impaired Mitochondrial Function in Contracting Gastrocnemius Muscle of Goto-Kakizaki Diabetic Rats In Vivo. PLoS One 2015;10:e0129579.
102. Liu Y, Mei X, Li J, Lai N, Yu X. Mitochondrial function assessed by 31 P MRS and BOLD MRI in non obese type 2 diabetic rats. Physiol Rep 2016;4:e12890.
103. Schmid AI, Schewzow K, Fiedler GB, Goluch S, Laistler E, Wolzt M, Moser E, Meyerspeer M. Exercising calf muscle T2* changes correlate with pH, PCr recovery and maximum oxidative phosphorylation. NMR Biomed 2014;27:553-60.
104. Parasoglou P, Xia D, Chang G, Regatte RR. Dynamic three-dimensional imaging of phosphocreatine recovery kinetics in the human lower leg muscles at 3T and 7T: a preliminary study. NMR Biomed 2013;26:348-56.
105. Shah PK, Ye F, Liu M, Jayaraman A, Baligand C, Walter G, Vandenborne K. In vivo (31)P NMR spectroscopy assessment of skeletal muscle bioenergetics after spinal cord contusion in rats. Eur J Appl Physiol 2014;114:847-58.
106. van den Broek NM, Ciapaite J, Nicolay K, Prompers JJ. Comparison of in vivo postexercise phosphocreatine recovery and resting ATP synthesis flux for the assessment of skeletal muscle mitochondrial function. Am J Physiol Cell Physiol 2010;299:C1136-43.
107. Ernst RR, Anderson WA. Application of Fourier Transform Spectroscopy to Magnetic Resonance. Rev Sci Instrum 1966;37:93.
108. Forsén S, Hoffman R. Study of Moderatly Rapid Chamical Exchange Reactions by Means of Nuclear Magnetic Double Resonance. J Chem Phys 1963;39:2892-901.
109. Brown TR, Ogawa S. 31P nuclear magnetic resonance kinetic measurements on adenylate kinase. Proc Natl Acad Sci U S A 1977;74:3627-31.
110. Brown TR, Ugurbil K, Shulman RG. 31P nuclear magnetic resonance measurements of ATPase kinetics in aerobic Escherichia coli cells. Proc Natl Acad Sci U S A 1977;74:5551-3.
111. Brown TR, Gadian DG, Garlick PB, Radda GK, Seeley PJ, Styles P. Creatine kinase activities in skeletal and cardiac muscle measured by saturation transfer NMR. Front Biol Energ 1978;2:1341-9.
112. Balaban RS, Kantor HL, Ferretti JA. In vivo flux between phosphocreatine and adenosine triphosphate determined by two-dimensional phosphorous NMR. J Biol Chem 1983;258:12787-9.
113. Kingsley-Hickman PB, Sako EY, Mohanakrishnan P, Robitaille PM, From AH, Foker JE, Uğurbil K. 31P NMR studies of ATP synthesis and hydrolysis kinetics in the intact myocardium. Biochemistry 1987;26:7501-10.
114. Robitaille PM, Merkle H, Sako E, Lang G, Clack RM, Bianco R, From AH, Foker J, Uğurbil K. Measurement of ATP synthesis rates by 31P-NMR spectroscopy in the intact myocardium in vivo. Magn Reson Med 1990;15:8-24.
115. Kingsley-Hickman PB, Sako EY, Uğurbil K, From AH, Foker JE, Fokers JE, Sakoz Y, Fromll HL. 31P NMR measurement of mitochondrial uncoupling in isolated rat hearts. J Biol Chem 1990;265:1545-50.
116. Leibfritz D, Dreher W. Magnetization transfer MRS. NMR Biomed 2001;14:65-76.
117. Ingwall JS. Phosphorus nuclear magnetic resonance

spectroscopy of cardiac and skeletal muscles. Am J Physiol 1982;242:H729-44.
118. Thoma WJ, Uğurbil K, Uğurbil K. Saturation-transfer studies of ATP-Pi exchange in isolated perfused rat liver. Biochim Biophys Acta 1987;893:225-31.
119. Matthews PM, Bland JL, Gadian DG, Radda GK. The steady-state rate of ATP synthesis in the perfused rat heart measured by 31P NMR saturation transfer. Biochem Biophys Res Commun 1981;103:1052-9.
120. Kemp GJ. The interpretation of abnormal 31P magnetic resonance saturation transfer measurements of Pi/ATP exchange in insulin-resistant skeletal muscle. Am J Physiol Endocrinol Metab 2008;294:E640-2; author reply E643-4.
121. Du F, Zhu XH, Qiao H, Zhang X, Chen W. Efficient in vivo 31P magnetization transfer approach for noninvasively determining multiple kinetic parameters and metabolic fluxes of ATP metabolism in the human brain. Magn Reson Med 2007;57:103-14.
122. Mlynárik V, Kasparová S, Liptaj T, Dobrota D, Horecký J, Belan V. Creatine kinase reaction rates in rat brain during chronic ischemia. MAGMA 1998;7:162-5.
123. McConnell HM. Reaction Rates by Nuclear Magnetic Resonance. J Chem Phys 1958;28:430.
124. Wang CY, Liu Y, Huang S, Griswold MA, Seiberlich N, Yu X. (31) P magnetic resonance fingerprinting for rapid quantification of creatine kinase reaction rate in vivo. NMR Biomed 2017;30:e3786.
125. From AH, Ugurbil K. Standard magnetic resonance-based measurements of the Pi→ATP rate do not index the rate of oxidative phosphorylation in cardiac and skeletal muscles. Am J Physiol Cell Physiol 2011;301:C1-11.
126. Balaban RS, Koretsky AP. Interpretation of 31P NMR saturation transfer experiments: what you can't see might confuse you. Focus on "Standard magnetic resonance-based measurements of the Pi→ATP rate do not index the rate of oxidative phosphorylation in cardiac and skeletal muscles. Am J Physiol Cell Physiol 2011;301:C12-5.
127. Degani H, Laughlin M, Campbell S, Shulman RG. Kinetics of creatine kinase in heart: a 31P NMR saturation- and inversion-transfer study. Biochemistry 1985;24:5510-6.
128. Buehler T, Kreis R, Boesch C. Comparison of 31P saturation and inversion magnetization transfer in human liver and skeletal muscle using a clinical MR system and surface coils. NMR Biomed 2015;28:188-99.
129. Ren J, Yang B, Sherry a D, Malloy CR. Exchange kinetics by inversion transfer: Integrated analysis of the phosphorus metabolite kinetic exchanges in resting human skeletal muscle at 7 T. Magn Reson Med 2015;73:1359-69.
130. Ren J, Sherry AD, Malloy CR. Amplification of the effects of magnetization exchange by (31) P band inversion for measuring adenosine triphosphate synthesis rates in human skeletal muscle. Magn Reson Med 2015;74:1505-14.
131. Bottomley PA, Ouwerkerk R, Lee RF, Weiss RG. Four-angle saturation transfer (FAST) method for measuring creatine kinase reaction rates in vivo. Magn Reson Med 2002;47:850-63.
132. Schär M, El-Sharkawy AM, Weiss RG, Bottomley PA. Triple repetition time saturation transfer (TRiST) 31P spectroscopy for measuring human creatine kinase reaction kinetics. Magn Reson Med 2010;63:1493-501.
133. Schär M, Gabr RE, El-Sharkawy AM, Steinberg A, Bottomley PA, Weiss RG. Two repetition time saturation transfer (TwiST) with spill-over correction to measure creatine kinase reaction rates in human hearts. J Cardiovasc Magn Reson 2015;17:70.
134. Xiong Q, Du F, Zhu X, Zhang P, Suntharalingam P, Ippolito J, Kamdar FD, Chen W, Zhang J. ATP production rate via creatine kinase or ATP synthase in vivo: a novel superfast magnetization saturation transfer method. Circ Res 2011;108:653-63.
135. Bresnen A, Duong TQ. Brain high-energy phosphates and creatine kinase synthesis rate under graded isoflurane anesthesia: An in vivo (31) P magnetization transfer study at 11.7 tesla. Magn Reson Med 2015;73:726-30.
136. Clarke WT, Robson MD, Neubauer S, Rodgers CT. Creatine kinase rate constant in the human heart measured with 3D-localization at 7 tesla. Magn Reson Med 2017;78:20-32.
137. Tušek Jelenc M, Chmelík M, Bogner W, Krššák M, Trattnig S, Valkovič L. Feasibility and repeatability of localized 31 P-MRS four-angle saturation transfer (FAST) of the human gastrocnemius muscle using a surface coil at 7 T. NMR Biomed 2016;29:57-65.
138. Ma D, Gulani V, Seiberlich N, Liu K, Sunshine JL, Duerk JL, Griswold MA. Magnetic resonance fingerprinting. Nature 2013;495:187-92.
139. Jiang Y, Ma D, Seiberlich N, Gulani V, Griswold MA. MR fingerprinting using fast imaging with steady state precession (FISP) with spiral readout. Magn Reson Med 2015;74:1621-31.
140. Moonen CT, von Kienlin M, van Zijl PC, Cohen J, Gillen J, Daly P, Wolf G. Comparison of Single-shot Localization Methods (STEAM and PRESS) for In Vivo Proton NMR Spectroscopy. NMR Biomed 1989;2:201-8.
141. Lamb HJ, Doornbos J, den Hollander JA, Luyten

PR, Beyerbacht HP, van der Wall EE, de Roos A. Reproducibility of human cardiac 31P-NMR spectroscopy. NMR Biomed 1996;9:217-27.
142. Luyten PR, Groen JP, Vermeulen JW, den Hollander JA. Experimental approaches to image localized human 31P NMR spectroscopy. Magn Reson Med 1989;11:1-21.
143. Sprott H, Rzanny R, Reichenbach JR, Kaiser WA, Hein G, Stein G. 31P magnetic resonance spectroscopy in fibromyalgic muscle. Rheumatology (Oxford) 2000;39:1121-5.
144. Bakermans AJ, Abdurrachim D, van Nierop BJ, Koeman A, van der Kroon I, Baartscheer A, Schumacher CA, Strijkers GJ, Houten SM, Zuurbier CJ, Nicolay K, Prompers JJ. In vivo mouse myocardial 31P MRS using three-dimensional image-selected in vivo spectroscopy (3D ISIS): Technical considerations and biochemical validations. NMR Biomed 2015;28:1218-27.
145. Chmelik M, Považan M, Krššák M, Gruber S, Tkačov M, Trattnig S, Bogner W. In vivo 31P magnetic resonance spectroscopy of the human liver at 7T: An initial experience. NMR Biomed 2014;27:478-85.
146. Kitagawa A, Saeki M, Imamura K, Ohashi K, Ishikawa T, Nakajima H, Takagi M. 31P-MR spectroscopy of bone and soft tissue lesions. Nihon Igaku Hoshasen Gakkai Zasshi 1995;55:1017-24.
147. Parasoglou P, Xia D, Chang G, Convit A, Regatte RR. Three-dimensional mapping of the creatine kinase enzyme reaction rate in muscles of the lower leg. NMR Biomed 2013;26:1142-51.
148. Parasoglou P, Xia D, Chang G, Regatte RR. Three-dimensional saturation transfer 31P-MRI in muscles of the lower leg at 3.0 T. Sci Rep 2014;4:5219.
149. Chao H, Bowers JL, Holtzman D, Mulkern RV. RARE imaging of PCr in human forearm muscles. J Magn Reson Imaging 1997;7:1048-55.
150. Greenman RL, Elliott MA, Vandenborne K, Schnall MD, Lenkinski RE. Fast imaging of phosphocreatine using a RARE pulse sequence. Magn Reson Med 1998;39:851-4.
151. Greenman RL. Quantification of the 31P metabolite concentration in human skeletal muscle from RARE image intensity. Magn Reson Med 2004;52:1036-42.
152. Greenman RL, Axel L, Ferrari VA, Lenkinski RE. Fast Imaging of Phosphocreatine in the Normal Human Myocardium Using a Three-Dimensional RARE Pulse Sequence at 4 Tesla. J Magn Reson Imaging 2002;15:467-72.
153. Greenman RL, Smithline HA. The Feasibility of Measuring Phosphocreatine Recovery Kinetics in Muscle Using Single-Shot 31 P RARE MRI Sequence. Acad Radiol 2011;18:917-23.
154. Greenman RL, Wang X, Smithline HA. Simultaneous acquisition of phosphocreatine and inorganic phosphate images for Pi:PCr ratio mapping using a RARE sequence with chemically selective interleaving. Magn Reson Imaging 2011;29:1138-44.
155. Lu A, Atkinson IC, Zhou XJ, Thulborn KR. PCr/ATP ratio mapping of the human head by simultaneously imaging of multiple spectral peaks with interleaved excitations and flexible twisted projection imaging readout trajectories at 9.4 T. Magn Reson Med 2013;69:538-44.
156. Schmid AI, Meyerspeer M, Robinson SD, Goluch S, Wolzt M, Fiedler GB, Bogner W, Laistler E, Krššák M, Moser E, Trattnig S, Valkovič L. Dynamic PCr and pH Imaging of Human Calf Muscles During Exercise and Recovery Using 31P Gradient-Echo MRI at 7 Tesla. Magn Reson Med 2016;75:2324-31.
157. Brown TR, Kincaid BM, Ugurbil K. NMR chemical shift imaging in three dimensions. Proc Natl Acad Sci U S A 1982;79:3523-6.
158. Pykett IL, Rosen BR. Nuclear magnetic resonance: in vivo proton chemical shift imaging. Work in progress. Radiology 1983;149:197-201.
159. Schlemmer HP, Sawatzki T, Sammet S, Dornacher I, Bachert P, van Kaick G, Waldherr R, Seitz HK. Hepatic phospholipids in alcoholic liver disease assessed by proton-decoupled 31P magnetic resonance spectroscopy. J Hepatol 2005;42:752-9.
160. Forbes SC, Slade JM, Francis RM, Meyer RA. Comparison of oxidative capacity among leg muscles in humans using gated 31P 2-D chemical shift imaging. NMR Biomed 2009;22:1063-71.
161. Vyhnanovská P, Dezortová M, Herynek V, Táborský P, Viklický O, Hájek M. In vivo 31P MR spectroscopy of human kidney grafts using the 2D-chemical shift imaging method. Transplant Proc 2011;43:1570-5.
162. Mareci TH, Brooker HR. High-resolution magnetic resonance spectra from a sensitive region defined with pulsed field gradients. J Magn Reson 1984;57:157-63.
163. Mareci TH, Brooker HR. Essential considerations for spectral localization using indirect gradient encoding of spatial information. J Magn Reson 1991;92:229-46.
164. Maudsley AA, Matson GB, Hugg JW, Weiner MW. Reduced phase encoding in spectroscopic imaging. Magn Reson Med 1994;31:645-51.
165. Ponder SL, Twieg DB. A Novel Sampling Method for 31P Spectroscopic Imaging with Improved Sensitivity,

Resolution, and Sidelobe Suppression. J Magn Reson B 1994;104:85-8.
166. Hendrich K, Hu X, Menon RS, Merkle H, Camarata P, Heros R, Uğurbil K. Spectroscopic imaging of circular voxels with a two-dimensional Fourier-series window technique. J Magn Reson B 1994;105:225-32.
167. Chmelík M, Schmid AI, Gruber S, Szendroedi J, Krssák M, Trattnig S, Moser E, Roden M. Three-dimensional high-resolution magnetic resonance spectroscopic imaging for absolute quantification of 31P metabolites in human liver. Magn Reson Med 2008;60:796-802.
168. Purvis LA, Clarke WT, Valkovič L, Levick C, Pavlides M, Barnes E, Cobbold JF, Robson MD, Rodgers CT. Phosphodiester content measured in human liver by in vivo 31P MR spectroscopy at 7 tesla. Magn Reson Med 2017;78:2095-105.
169. Pohmann R, Von Kienlin M. Accurate phosphorus metabolite images of the human heart by 3D acquisition-weighted CSI. Magn Reson Med 2001;45:817-26.
170. Posse S, DeCarli C, Le Bihan D. Three-dimensional echo-planar MR spectroscopic imaging at short echo times in the human brain. Radiology 1994;192:733-8.
171. Adalsteinsson E, Irarrazabal P, Topp S, Meyer C, Macovski A, Spielman DM. Volumetric spectroscopic imaging with spiral-based k-space trajectories. Magn Reson Med 1998;39:889-98.
172. Schirda CV, Tanase C, Boada FE. Rosette spectroscopic imaging: Optimal parameters for alias-free, high sensitivity spectroscopic imaging. J Magn Reson Imaging 2009;29:1375-85.
173. Korzowski A, Bachert P. High-resolution (31) P echo-planar spectroscopic imaging in vivo at 7T. Magn Reson Med 2017. [Epub ahead of print]. doi: 10.1002/mrm.26785.
174. Valkovič L, Chmelík M, Meyerspeer M, Gagoski B, Rodgers CT, Krššák M, Andronesi OC, Trattnig S, Bogner W. Dynamic 31P-MRSI using spiral spectroscopic imaging can map mitochondrial capacity in muscles of the human calf during plantar flexion exercise at 7 T. NMR Biomed 2016;29:1825-34.
175. Pohmann R, von Kienlin M, Haase A. Theoretical evaluation and comparison of fast chemical shift imaging methods. J Magn Reson 1997;129:145-60.
176. Speck O, Scheffler K, Hennig J. Fast 31P chemical shift imaging using SSFP methods. Magn Reson Med 2002;48:633-9.
177. Leupold J, Wieben O, Månsson S, Speck O, Scheffler K, Petersson JS, Hennig J. Fast chemical shift mapping with multiecho balanced SSFP. MAGMA 2006;19:267-73.
178. Lam F, Liang ZP. A subspace approach to high-resolution spectroscopic imaging. Magn Reson Med 2014;71:1349-57.
179. Lam F, Ning Q, Liu Q, Johnson CL, Liang Z. High-Resolution Dynamic 31P-MRSI Using High-Order Partially Separable Functions. Proc Intl Soc Mag Reson Med 2016;24:4-6.
180. Ma C, Lam F, Ning Q, Johnson CL, Liang ZP. High-resolution (1) H-MRSI of the brain using short-TE SPICE. Magn Reson Med 2017;77:467-79.
181. Ma C, Clifford B, Liu Y, Gu Y, Lam F, Yu X, Liang ZP. High-resolution dynamic 31P-MRSI using a low-rank tensor model. Magn Reson Med 2017;78:419-28.
182. Griswold MA, Jakob PM, Heidemann RM, Nittka M, Jellus V, Wang J, Kiefer B, Haase A. Generalized Autocalibrating Partially Parallel Acquisitions (GRAPPA). Magn Reson Med 2002;47:1202-10.
183. Pruessmann KP, Weiger M, Scheidegger MB, Boesiger P. SENSE: Sensitivity encoding for fast MRI. Magn Reson Med 1999;42:952-62.
184. Sodickson DK, Manning WJ. Simultaneous acquisition of spatial harmonics (SMASH): Fast imaging with radiofrequency coil arrays. Magn Reson Med 1997;38:591-603.
185. Lustig M, Donoho D, Pauly JM. Sparse MRI: The application of compressed sensing for rapid MR imaging. Magn Reson Med 2007;58:1182-95.
186. Feng Y, Gordon JW, Shin PJ, von Morze C, Lustig M, Larson PE, Ohliger MA, Carvajal L, Tropp J, Pauly JM, Vigneron DB. Development and testing of hyperpolarized 13C MR calibrationless parallel imaging. J Magn Reson 2016;262:1-7.
187. Cao P, Shin PJ, Park I, Najac C, Marco-Rius I, Vigneron DB, Nelson SJ, Ronen SM, Larson PE. Accelerated high-bandwidth MR spectroscopic imaging using compressed sensing. Magn Reson Med 2016;76:369-79.
188. Parasoglou P, Feng L, Xia D, Otazo R, Regatte RR. Rapid 3D-imaging of phosphocreatine recovery kinetics in the human lower leg muscles with compressed sensing. Magn Reson Med 2012;68:1738-46.

Cite this article as: Liu Y, Gu Y, Yu X. Assessing tissue metabolism by phosphorous-31 magnetic resonance spectroscopy and imaging: a methodology review. Quant Imaging Med Surg 2017;7(6):707-726. doi: 10.21037/qims.2017.11.03

